JOURNAL OF APPLIED ELECTROCHEMISTRY 9 (1979) 43–53

Inhibited zinc electrodeposition: electrode kinetics and deposit morphology

J. BRESSAN, R. WIART

Groupe de Recherche no. 4 du CNRS 'Physique des Liquides et Electrochimie', associé à l'Université Pierre et Marie Curie, 4 place Jussieu, 75230 Parix Cedex 05

Received 1 February 1978

The electrode kinetics of spongy and dendritic zinc deposition were studied in the presence of three inhibitors (lead acetate, tetrabutylammonium bromide and benzalacetone). It was shown that these additives increase the cathodic overvoltage, decrease the current efficiency, eliminate multiple steady states in acid electrolytes, and modify the impedance diagrams. Such changes in electrode kinetics were interpreted in terms of weaker autocatalytic adsorption of metal cations and enhanced hydrogen adsorption. It was also shown that a pH decrease had a similar effect on these reaction rates. It was concluded from very low frequency impedance measurements that the additives give rise to an accelerated nucleation rate ensuring a faster renewal of active growth sites.

1. Introduction

An increase in current density during zinc electrodeposition leads to progressively spongy, compact and dendritic deposits both in alkaline and acid media. It is well known that some additives are able to widen the range of current densities in which compact deposits are formed [1–8]. With lead acetate ($PbAc_2$), the inhibiting effect on the irregular growth of electrodeposits is accompanied by significant changes in the reaction kinetics. We have shown previously [9] that current–potential curves and impedance diagrams are clearly modified when $PbAc_2$ is present in the electrolyte.

This paper shows that the correlation can be generalized, and lead acetate is compared with two other inhibitors (tetrabutylammonium bromide, NBu_4Br and benzalacetone, ϕ–CH=CH–$COCH_3$). Precise details are given of the inhibition mechanism of zinc electrocrystallization, as a result of both hydrogen adsorption and the presence of additive in the electrolyte. To this end a recent model for zinc electrocrystallization is used. This model is based on a detailed description of the interfacial reactions, and on the localization of these reactions on particular sites on the metal surface [10, 11].

2. Experimental

The electrolytic cell has been described previously [9]. Three electrolytes commonly used in the zinc industry were investigated:

(a) The Leclanché cell electrolyte: 2·67 M NH_4Cl, 0·72 M $ZnCl_2$, pH adjusted to 5·2 with NH_4OH.

(b) An alkaline electrolyte used in accumulators: 7 M KOH, 0·5 M ZnO.

(c) An acid sulphate electrolyte utilized in zinc metallurgy: 1·5 M $ZnSO_4$, 1 M Na_2SO_4.

High purity NBu_4Br (Fluka) was used as a well-known inhibitor of dendritic zinc growth in alkali [4]. Benzalacetone is an industrial additive used to obtain bright zinc deposits in acid media [12].

Current–potential data and impedance measurements were made galvanostatically as described previously [9]. The ohmic drop was measured using an interrupter method [13, 14] and analogically compensated [15].

In order to prepare reproducible zinc electrodeposits it was necessary not to dry the electrode before deposition, so that no weighing could be made before electrolysis. Consequently, efficiency measurements were performed using a copper pastille substrate (Johnson–Matthey, 99·999%) maintained in contact with the rotating stainless

steel cylinder by a thermoretractable plastic tube.

After electrolysis the deposit-bearing substrate was removed, and the deposit weight found by measuring the weight of the substrate before and after dissolution of the deposit in 50% HCl. Before each weighing the sample was washed with ethyl acetate and vacuum dried. The weighings, performed on an electronic balance (Sartorius), allowed a determination of the efficiency (η) to within 0·5%.

3. Results

3.1. *Deposit morphology*

It has been observed that the addition of small amounts of NBu_4Br to the Leclanché cell electrolyte increases the range of current densities leading to compact deposits.

At low current densities the formation of spongy deposits is progressively inhibited with increasing NBu_4Br concentration, which favours the formation of compact deposits over the whole electrode surface. As an example for an electrode rotating at 2000 rev min^{-1}, a compact deposit is observed when the additive concentration reaches 5×10^{-5} M (Fig. 1a). The influence of NBu_4Br on deposit morphology is stronger than in the case of $PbAc_2$, which only gives regions of compact deposit distributed over the electrode surface [9].

At high current densities the dendritic growth is also inhibited. A compact deposit is formed on an electrode rotating at 2000 rev min^{-1} as soon as the NBu_4Br concentration is greater than 5×10^{-4} M (Fig. 1b). The deposits exhibit the same morphology for additive concentrations between 5×10^{-4} M and 5×10^{-3} M. Similar deposits have also been observed in alkaline media [4].

3.2. *Current efficiency*

At low current densities, the presence of $PbAc_2$ in the electrolyte is known to decrease the current efficiency during zinc electrocrystallization [8]. Similarly, the addition of benzalacetone tends to make the bath more hydrogenating [12]. The addition of NBu_4Br to the Lechlanché cell electrolyte also leads to an efficiency decrease which is more marked at low current densities. Efficiency versus current curves are given in Fig. 2 for an electrolyte without any additive (Curve 1) and with 5×10^{-4} M NBu_4Br (Curve 2).

3.3. *Current–potential curves and impedance diagrams*

The influence of additives on the current–potential curves and impedance diagrams has been investigated in both acid and alkaline media.

For the inhibitor-free Leclanché cell electrolyte, the current–potential curve is S-shaped confirming the existence of multiple steady states (Fig. 3, Curve 1). As with $PbAc_2$, the addition of NBu_4Br eliminates these. The curves become single valued and shifted towards more cathodic potentials as the additive concentration is increased (Fig. 3).

Similar curves are observed in an alkaline medium (Fig. 4), but the shift is far greater (e.g. at a NBu_4Br concentration of 5×10^{-4} M and a current of 10 mA, the increase in cathodic polarization is seen to be 70 mV instead of 45 mV in acidic solution).

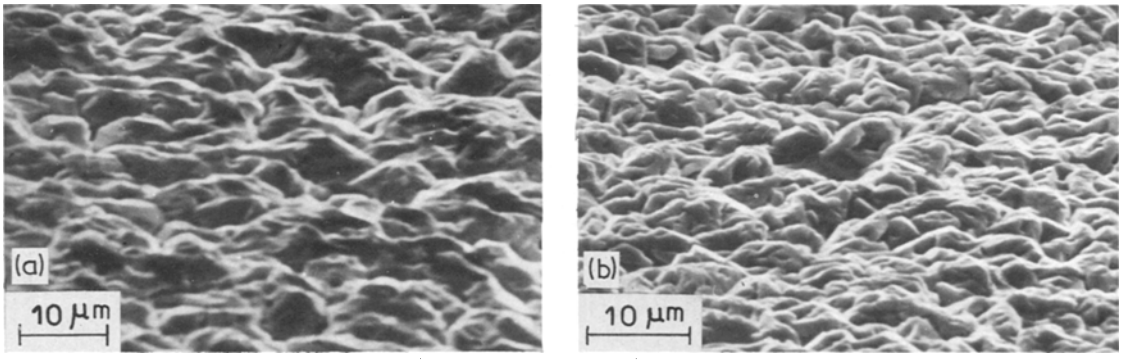

Fig. 1. Zinc deposits prepared in a Leclanché cell electrolyte with 5×10^{-4} M NBu_4Br (electron rotation speed 2000 rev min^{-1}; area 0·28 cm^2). Current density: (a) 3·5 mA cm^{-2}; (b) 350 mA cm^{-2}.

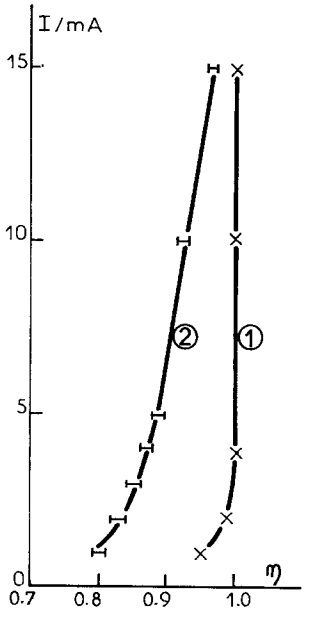

Fig. 2. Relationship between the current efficiency η and the current I. Electrolyte: NH_4Cl 2·67 M, $ZnCl_2$ 0·72 M, pH = 5·2. Rotating disk electrode (2000 rev min^{-1}; area 0·28 cm^2). Curve 1: without inhibitor. Curve 2: with 5 × 10^{-4} M NBu_4Br.

The impedance is also modified on addition of NBu_4Br to the electrolyte. The behaviour is similar to that observed for $PbAc_2$.

An impedance diagram for the Leclanché cell electrolyte is shown in Fig. 3b (obtained at point A on Fig. 3a). An inductive loop (4 × 10^{-3} Hz–30 Hz), a capacitive loop (30 Hz–80 Hz) and a second inductive loop (80 Hz–200 Hz) are observed. This contrasts with the inductive impedance characterized by three time constants observed when no inhibitor is present [16] (see also Fig. 6).

NBu_4Br also affects the low frequency impedance in alkaline solutions. Fig. 4b shows that an inductive loop (0·063 Hz–1·6 Hz), a capacitive loop (1·6 Hz–16 Hz) and an inductive loop (16 Hz–100 Hz) are still obtained. These diagrams are observed for concentrations from 5 × 10^{-5} M to 5 × 10^{-4} M NBu_4Br, and for currents between 5–15 mA in both acidic and alkaline media.

Though NBu_4Br and $PbAc_2$ similarly affect the low frequency impedance, it is interesting to note that the frequency characteristic of the lowest frequency loop is higher with NBu_4Br (0·6 Hz)

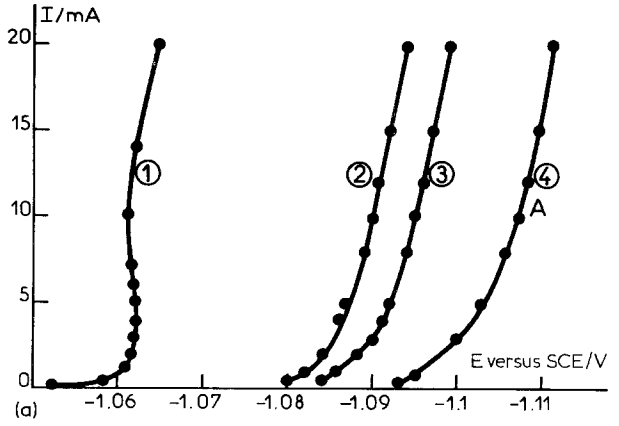

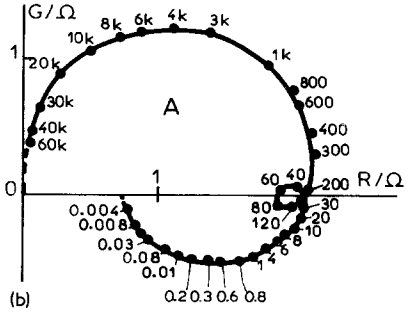

Fig. 3. (a) Steady state current–potential curves plotted for the Leclanché cell electrolyte with a rotating disk electrode (1000 rev min^{-1}; area 0·2 cm^2). Concentration of NBu_4Br: 0 (Curve 1), 5 × 10^{-5} (Curve 2), 10^{-4} (Curve 3) and 5 × 10^{-4} M (Curve 4). (b) Complex impedance diagram $Z = R - jG$ corresponding to point A on Curve 4 (frequency in Hz).

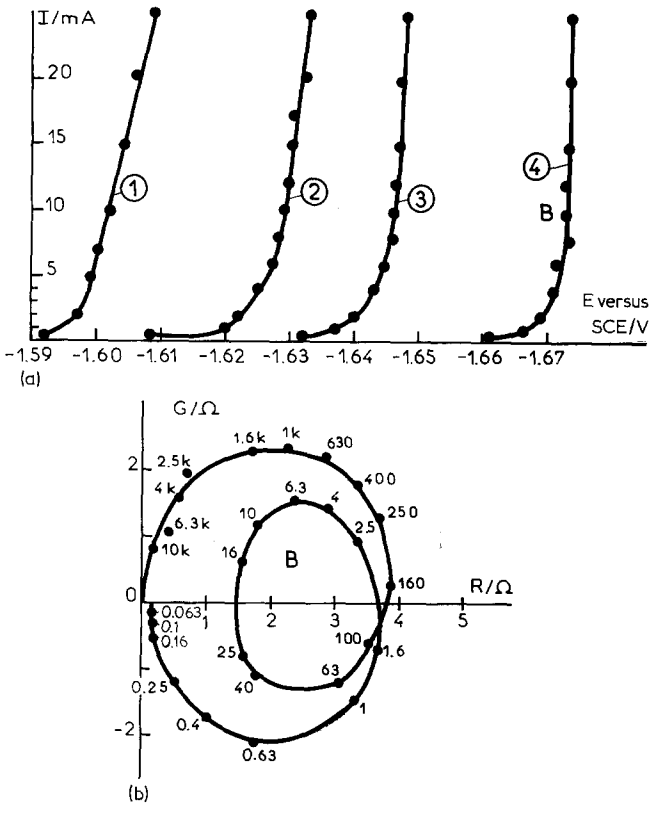

Fig. 4. (a) Steady state current–potential curves plotted for the alkaline zincate electrolyte: KOH 7 M, ZnO 0·5 M, with a rotating disk electrode (1500 rev min^{-1}; area 0·2 cm^2). Concentration of NBu_4Br: 0 (Curve 1), 5×10^{-5} (Curve 2), 10^{-4} (Curve 3), and 5×10^{-4} M (Curve 4). (b) Complex impedance diagram $Z = R - jG$ corresponding to point B on Curve 4 (frequency in Hz).

than with $PbAc_2$ (0·1 Hz) in both acid and alkali [9, 17].

At frequencies above 200 Hz, the impedance diagrams are semicircular and correspond to the double-layer capacitance (C_d) in parallel with the charge transfer resistance (R_t). The value of C_d is smaller by a factor of 4 or 5 in the presence of NBu_4Br, which is similar to the decrease obtained with $PbAc_2$ [9].

The addition of benzalacetone to the acid electrolyte modifies the electrode kinetics in the same manner as does NBu_4Br. Similar shifts in current–potential curves and changes in the low frequency impedance are observed (Fig. 5a). Fig. 5b (obtained at point C on Fig. 5a) shows successively inductive, capacitive and inductive loops in the ranges 0·004 Hz–30 Hz, 30 Hz–80 Hz and 80 Hz–200 Hz, respectively. The frequency characteristic of the lowest frequency loop has a value of 0·6 Hz which is the same as for NBu_4Br.

Hydrogen adsorption also inhibits the zinc electrocrystallization reaction and this effect is clearly observed in the acid sulphate electrolyte. A pH decrease makes the current–potential curve become single-valued and causes a shift to more cathodic potentials (Fig. 6a). The faradaic impedance is also notably modified (Figs. 6b and c taken at points D and E of Fig. 6a). At the lower pH only two inductive loops can be distinguished in the bandwidths 0–0·1 Hz and 0·1 Hz–40 Hz. The value of the double-layer capacitance (40 $\mu F\ cm^{-2}$) is not appreciably altered.

It has been shown previously in our laboratory [16] that the current efficiency falls with a decreasing pH as in the case of an additive in the electrolyte.

4. Discussion

The electrode kinetics and the spontaneous formation of irregular zinc deposits at low or high current densities can be explained in terms of a mechanism formulated in our laboratory [10, 11]. This reaction sequence, outlined below, enables a better understanding of how the kinetics of the interfacial processes are modified in the presence of an inhibitor.

We consider that a fraction, θ_1, of the electrode

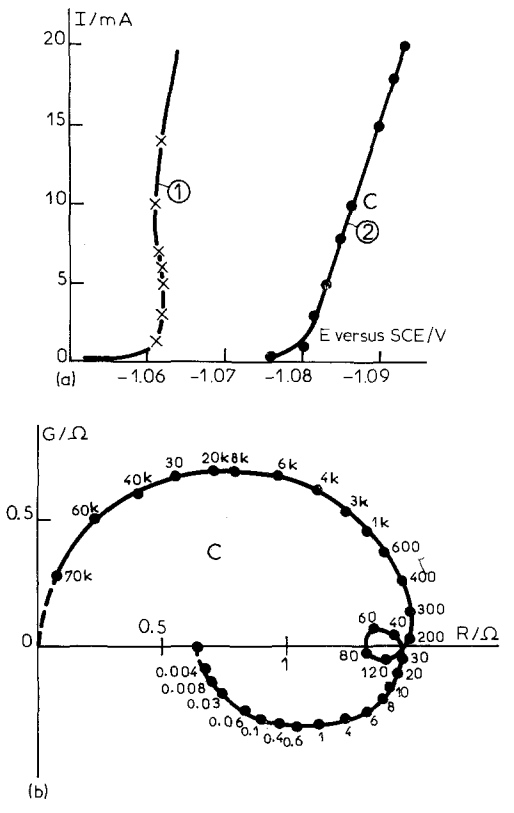

Fig. 5. (a) Steady state current–potential curves plotted for the Leclanché cell electrolyte. Rotating disk electrode (1000 rev min^{-1}; area 0·2 cm^2). Concentration of benzalacetone: 0 (Curve 1), 8 $cm^3 l^{-1}$ (Curve 2). (b) Complex impedance diagram $Z = R - jG$ corresponding to point C on Curve 2 (frequency in Hz).

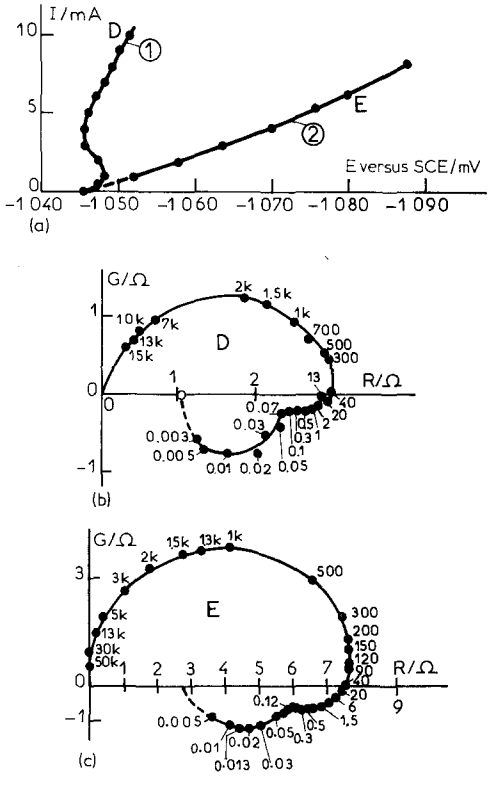

Fig. 6. (a) Steady state current–potential curves plotted for the acid sulphate solution: $ZnSO_4 \cdot 7\,H_2O$ 1·5 M, Na_2SO_4 1 M. Rotating disk electrode (2500 rev min^{-1}; area, 0·28 cm^2) pH = 4·3 (Curve 1), 2 (Curve 2). (b) and (c) Complex impedance diagrams $Z = R - jG$ corresponding to point D (b) on Curve 1 and point E (c) on Curve 2 (frequency in Hz).

surface is covered with adsorbed hydrogen, H_{ads}, formed by

$$H^+ + e \xrightarrow{A_1} H_{ads} \qquad (1)$$

and partially consumed during hydrogen evolution

$$H^+ + H_{ads} + e \xrightarrow{A_2} H_2. \qquad (2)$$

In order to describe zinc electrocrystallization, two types of intermediates are implied:

(a) The adions $Zn(I)_{ads}$ which are weakly bonded to the metal and able to diffuse along the electrode surface. These cover a fraction, θ_2, of the I sites belonging to planes or zones with lattice imperfections. The following reactions proposed previously [16] may occur on such sites

$$Zn(II) + Zn(I)_{ads} + e \underset{A_3'}{\overset{A_3}{\rightleftarrows}} 2Zn(I)_{ads} \qquad (3)$$

$$Zn(I)_{ads} + H_{ads} \xrightarrow{A_4} Zn + H^+ \qquad (4)$$

$$Zn(I)_{ads} + e \xrightarrow{A_5} Zn \qquad (5)$$

$$Zn(II) + e \xrightarrow{A_6} Zn(I)_{ads}. \qquad (6)$$

The cations are adsorbed via Reaction 6 and the autocatalytic Reaction 3. Reactions 4 and 5 describe the incorporation of adions on growth sites. These sites are provided by defects and consequently require no renewal.

(b) The growth sites Zn* which occupy a fraction, θ_3, of the II sites belonging to the growth steps of a perfect lattice. These sites are generated by the nucleation reaction

$$Zn(I)_{ads} + e \xrightarrow{A_7} Zn^*. \qquad (7)$$

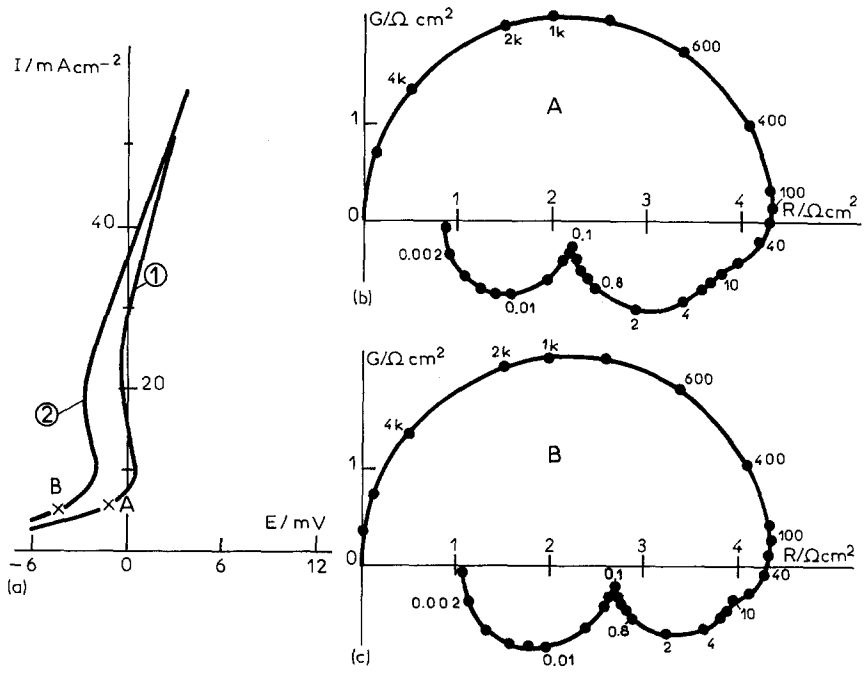

Fig. 7. (a) Current density–potential curves simulated: Curve 1, from Reactions 1–9, with normalized rate constants A_i and coefficients b_i, given elsewhere [8]; Curve 2 from the same set of reactions plus Reaction 10 with $A_{10} = A_7$. (b) and (c) Impedance diagrams simulated at point A (b) on Curve 1 and point B (c) on Curve 2 with $C_d = 50\,\mu F\,cm^{-2}$, $\beta_1 = 10\beta_2 = \beta_3 = 2{\cdot}7 \times 10^{-9}\,mol\,cm^{-2}$ (frequency in Hz).

The intermediates Zn* are assumed to catalyse reaction 8 which is an overall process

$$Zn^* + Zn(II) + 2e \xrightarrow{A_8} Zn + Zn^*. \qquad (8)$$

This kind of charge transfer occurring on a self-propagating kink has already been proposed for silver [18] and iron [19] deposition.

At certain stages in the growth some kinks lose their activity

$$Zn^* \xrightarrow{A_9} Zn \qquad (9)$$

Reaction 3 has a pronounced effect on the morphology of deposits formed [10]. At high current densities, the autocatalytic formation of $Zn(I)_{ads}$ gives rise to a strong acceleration of the Zn* production rate. This leads to the formation of numerous nuclei which initiate dendritic growth. In contrast, at low current densities, both autocatalytic adsorption and surface diffusion of adions govern the formation of local peaks of current density. This leads to the growth of some packs of spongy deposit. Consequently, Reactions 1–9 allow a close correlation to be made between electrode kinetics and deposit morphology.

According to a classical method, material and electron balances written with simple assumptions (Langmuir isotherm, and electron transfer obeying Tafel's law) allow a simulation of current–potential curves and impedance diagrams [10]. Each Reaction i (where i = 1–9), is characterized by a normalized rate constant (A_i) proportional to its rate constant K_i, to the concentration of adsorbing cations, and to the maximum surface concentrations β_1, β_2 or β_3 of the reaction intermediates H_{ads}, $Zn(I)_{ads}$ or Zn* which react in this reaction. Each electrochemical reaction is also characterized by a transfer coefficient α_i (where $b_i = \alpha_i n_i F/RT$). Fig. 7 shows that with appropriate values of the normalized constants A_i, and parameters b_i, an S-shaped current–potential curve (Curve 1) and an impedance diagram with three inductive loops (Fig. 7b at point A on Fig. 7a) can be generated. The lowest frequency loop corresponds to the slow relaxation of θ_3 (i.e. of the concentration of active kinks, Zn*).

At low current densities, the simulated impedance diagrams (Fig. 7b) are distorted compared to the experimental results [16] (see also Fig. 6). The loop at frequencies lower than 0·1 Hz is smaller than the 0·1 Hz–10 Hz loop on Fig. 7b. This is not true of the experimental observations. This deficiency in the model can be remedied if we consider that Zn* formation occurs not only via Reaction 7, but also through

$$H_{ads} + Zn(I)_{ads} \xrightarrow{A_{10}} Zn^* + H^+ \qquad (10)$$

so assuming that H_{ads} favours nucleation. If Reactions 7 and 10 occur simultaneously and with approximately the same normalized rate constants, new plots are simulated. The S-shaped current–potential curve (Fig. 7a Curve 2) and impedance diagram (Fig. 7c taken at point B on Fig. 7a) now agree with experimental data in a current density range widened towards lower values. Thus it seems probable that nucleation occurs via the electrochemical step (Reaction 7) and the chemical reduction of adions (Reaction 10).

Considering now the case of a decreased Zn(II) concentration in the electrolyte (i.e. smaller normalized rate constants A_3, A_6 and A_8), then the simulated current–potential curve is shifted towards more cathodic potentials (Fig. 8a Curve 2) and the multiple steady states are eliminated. This is in agreement with experimental data [10]. The resultant impedance diagram (Fig. 8b taken at point C on Fig. 8a) has a capacitive loop between 100 Hz–20 Hz. Such a change has been observed with a sulphate electrolyte [10], though the measured amplitude of the capacitive loop was larger than the simulated one. It is possible to simulate a larger capacitive loop by considering that the reaction

$$Zn(I)_{ads} + Zn^* + e \xrightarrow{A_{11}} Zn^* + Zn \qquad (11)$$

which describes the discharge and incorporation of the adions $Zn(I)_{ads}$, would occur on the kinks.

If Reaction 8 is replaced by Reaction 11, the graphs in Fig. 8a Curve 3, and Fig. 8c (taken at point D on Fig. 8a) are generated. The capacitive

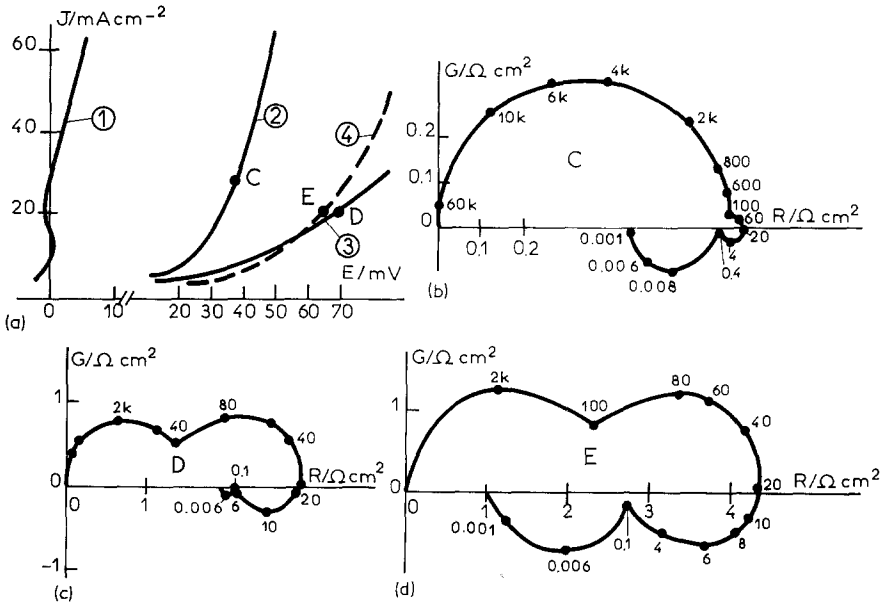

Fig. 8. Simulation of the influence of Zn(II) concentration on current density–potential curves with respect to an arbitrary origin and on impedance diagrams. (a) Curve 1, the same curve as Curve 1 in Fig. 7a; Curve 2, calculated from the same set of parameters as for Curve 1 by multiplying the Zn(II) concentration by 0·8; Curve 3, calculated by multiplying the Zn(II) concentration by 0·8, in the case where Reaction 8 has been replaced by Reaction 11 (A_{11} = 0·162 98 × 10^{-6} $cm^{-2}s^{-1}$ for $E = 0$; b_{11} = 19·3 V^{-1}); Curve 4, calculated by multiplying the Zn(II) concentration by 0·8 in the case where Reactions 8 and 11 occur simultaneously (A_8 = 0·8149 × 10^{-7} $cm^{-2}s^{-1}$ and A_{11} = 0·162 98 × 10^{-8} $cm^{-2}s^{-1}$ for $E = 0$). (b), (c) and (d) Impedance diagrams simulated at point C (b), D (c) and E (d) with the values of C_d, β_1, β_2, β_3 given in Fig. 7 (frequency in Hz).

loop is larger than on Fig. 8b but the lowest frequency inductive loop has become too small.

If we suppose that both Reactions 8 and 11 occur on the kinks, impedance diagrams closer to reality (Fig. 8d, taken at point E on Fig. 8a) can be simulated. It therefore seems likely that both the cations Zn(II) and adions $Zn(I)_{ads}$ are discharged on kinks.

However, the influence of an inhibitor on the electrode kinetics can be explained using the original reaction scheme without Reactions 10 and 11. As outlined below, Reactions 1–9 are sufficient to predict the changes of the impedance diagrams due to an inhibitor.

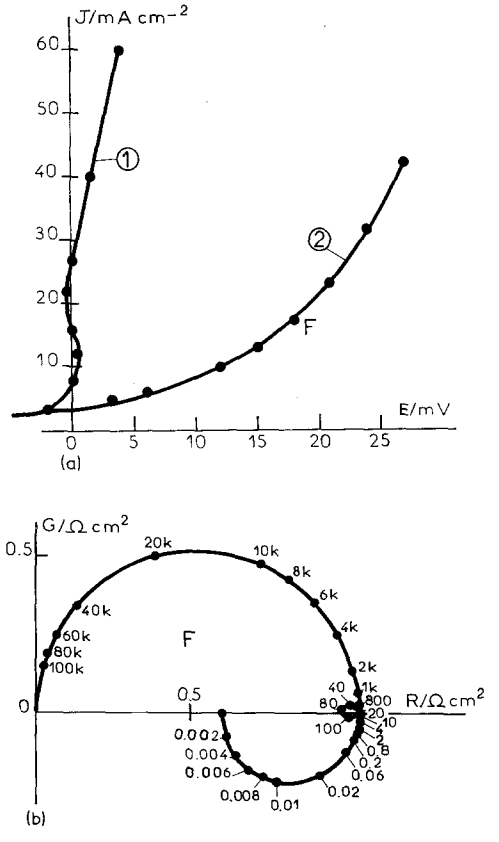

Fig. 9. Simulation of the influence of an additive on current density–potential curves and on impedance diagram. (a) Curve 1, the same curve as Curve 1 in Fig. 7a; Curve 2, calculated from the same set of parameters as for Curve 1 by multiplying A_3 by 0·9, A_7 and A_9 by 2 and changing b_1 from 5 to 38·6 V^{-1}, b_3 from 33·8 to 32 V^{-1} and b'_3 from 4·8 to 6·6 V^{-1}. (b) Impedance diagram simulated at point F on Curve 2 with $C_d = 10\,\mu F\,cm^{-2}$ (frequency in Hz).

4.1. *Influence of an additive*

The presence of an additive in the electrolyte increases the cathodic overvoltage, eliminates multiple steady states in acid media, diminishes the current efficiency and markedly alters impedance diagrams.

The single-valued current–potential curve obtained with an additive indicates that the autocatalytic Reaction 3 is slowed down. In addition, the shape of the impedance diagram suggests that hydrogen adsorption is stimulated. The deceleration of Reaction 3 and enhancement of Reaction 1 are expressed by a decrease in A_3 and b_3, and an increase in b_1. Fig. 9a, Curve 2 and impedance diagram (Fig. 9b, taken at point F on Fig. 9a) have been produced using these adjusted values. The relaxation frequencies on Fig. 9b conform with those experimentally obtained with $PbAc_2$, taking into account the decrease in double-layer capacity and an increase in the constants A_7 and A_9 due to the additive. These rate constants govern the slowest relaxation process and the characteristic frequency of this process has been shown, experimentally, to be dependent on the additive. Thus, the rate constants of Reactions 7 and 9, which correspond to the production and removal of Zn^*, are increased by an additive. These results indicate that the nucleation rate is multiplied by a factor of 10 in the presence of NBu_4Br or benzalacetone, whereas it is only doubled with $PbAc_2$.

Using the modified kinetic parameters of Reactions 1 and 3, it is possible to simulate variations of the product R_tI in agreement with experimental results. In the presence of an additive, R_tI is increased and remains a decreasing function of current (Fig. 10).

The same kinetic parameters lead to a simulated decrease in current efficiency for the zinc electrocrystallization process, as shown in Fig. 11a. This is similar to the experimentally observed diminution (Fig. 2).

Impedance diagrams for the additive-containing electrolyte exhibit a capacitive loop (between 80–20 Hz on the diagram simulated in Fig. 9). This is closely connected to a change in the variation of the partial coverages θ_1 (for H_{ads}), θ_2 (for $Zn(I)_{ads}$) and θ_3 (for Zn) with current density. The current density–partial coverage

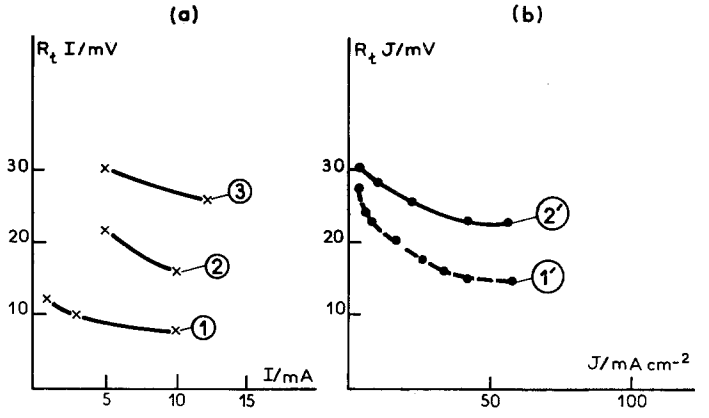

Fig. 10. Relationship between $R_t I$ and the current I. (a) Experimental results. Concentration of NBu_4Br: 0 (Curve 1), 5×10^{-5} (Curve 2) and 5×10^{-4} M (Curve 3). (b) Simulations. Curves 1' and 2' are obtained respectively with the same sets of parameters as for Curves 1 and 2 in Fig. 9a.

curves for θ_1 and θ_2 are shown in Figs. 11b and c, respectively. These were simulated using modified kinetic parameters for Reactions 1 and 3. In the presence of an additive (Curves 2), it can be seen that the electrode surface remains strongly blocked by H_{ads} (and consequently less covered by $Zn(I)_{ads}$) when the current increases. Hence the presence of the additive favours hydrogen adsorption at the electrode.

If Reactions 8 and 11 occur simultaneously on the electrode, the simulated impedance diagrams for an additive-containing electrolyte (Fig. 12) reveal the capacitive loop due to the additive, more clearly. This provides additional confirmation for the occurrence of Reaction 11 with Reaction 8 on the kinks.

4.2. *Influence of H^+*

It has been observed experimentally, that in a sulphate electrolyte a pH decrease shifts the current–potential curve towards more cathodic potentials, eliminates the multiple steady states, diminishes the current efficiency and modifies the inductive impedance. Thus acidification acts in the same direction as an additive.

Single-valued current–potential curves cannot be explained solely in terms of an increase in normalized rate constants for Reactions 1 and 2 which are proportional to H^+ concentration. However, if in addition, the autocatalytic Reaction 3 is slowed down by acidification, then the shapes of the current–potential curves and impedance diagrams can be satisfactorily simulated. In Fig. 13a, the current–potential Curve 2 and impedance diagram (Fig. 13b, taken at point G on Fig. 13a) have been generated by reducing b_3, and increasing A_1 and b_1 and also A_2 slightly. Thus, the addition of H^+ ions stimulates the hydrogen adsorption (Reaction 1) much more than hydrogen evolution (Reaction 2). This suggests that hydrogen evolution not only occurs via Reaction 2 (which should be

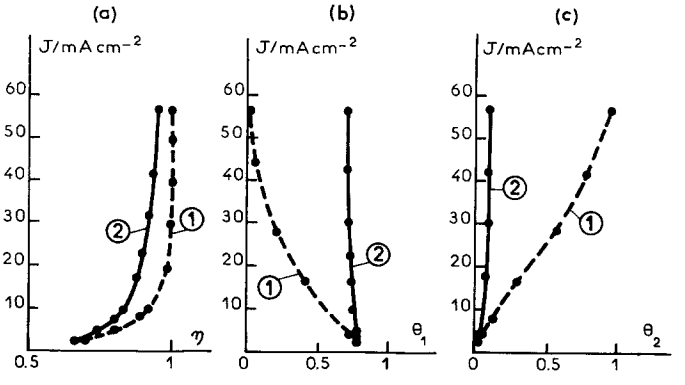

Fig. 11. Simulations of the relationships: (a) current density–efficiency; (b) current density–θ_1; (c) current density–θ_2. Curves 1 and 2 are obtained respectively with the same sets of parameters as for Curves 1 and 2 in Fig. 9a.

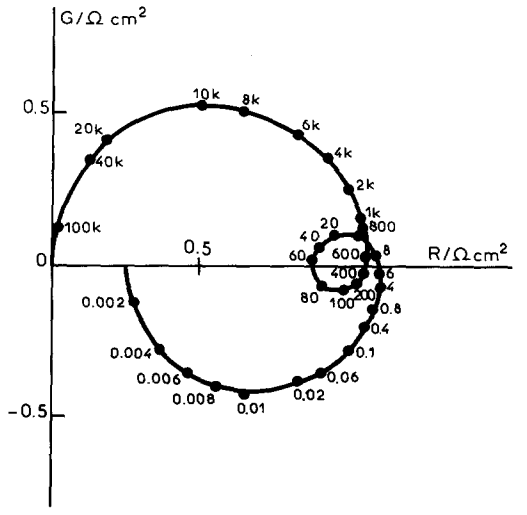

Fig. 12. Impedance diagram simulated for $E = 21$ mV (current density $(J) = 13$ mA cm^{-2}) with the same set of parameters as for Curve 2 in Fig. 9a, in the case where Reactions 8 and 11 occur simultaneously ($A_8 = 0{\cdot}8149 \times 10^{-7}$ cm^{-2} s^{-1} and $A_{11} = 0{\cdot}16298 \times 10^{-8}$ for $E = 0$).

activated in the same manner as Reaction 1), but also through a chemical recombination mechanism whose rate is not directly proportional to the concentration of H^+ in the electrolyte.

Unlike the case with an inhibitor, the slight increase in nucleation rate (Reaction 7) resulting from the cathodic shift of the current–potential curve, is sufficient to account for the value of the lowest relaxation frequency which remains close to 0·006 Hz. Hence the rate constant of Reaction 7 is probably not modified by an addition of H^+ ions.

Modifications to the kinetic parameters of Reactions 1, 2 and 3 allow us to predict, at a given current density, the increase in charge transfer resistance of about 10% which is observed experimentally with a pH decrease.

Fig. 14a shows that these modifications also account for the experimental decrease of current efficiency [16].

The relatively strong stimulation of hydrogen

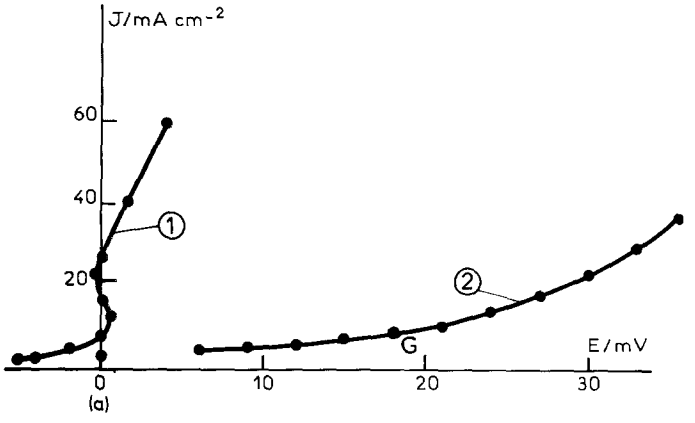

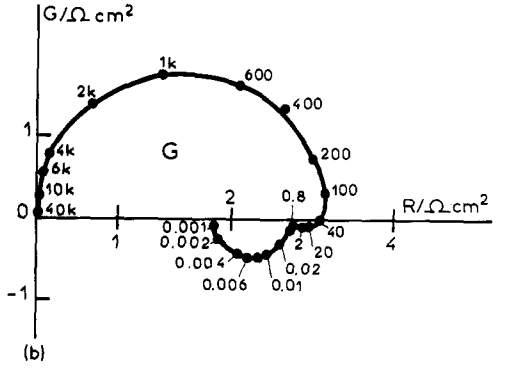

Fig. 13. Simulation of a pH decrease on current density–potential curves and on impedance diagrams. (a) Curve 1, the same curve as Curve 1 in Fig. 7a; Curve 2, calculated from the same set of parameters as for Curve 1 by multiplying A_1 by 10, b_1 by 5, A_2 by 2, and changing b_3 from 33·8 to 30 V^{-1} and b'_3 from 4·8 to 8·6 V^{-1}. (b) Impedance diagram simulated at point G on Curve 2 (frequency in Hz).

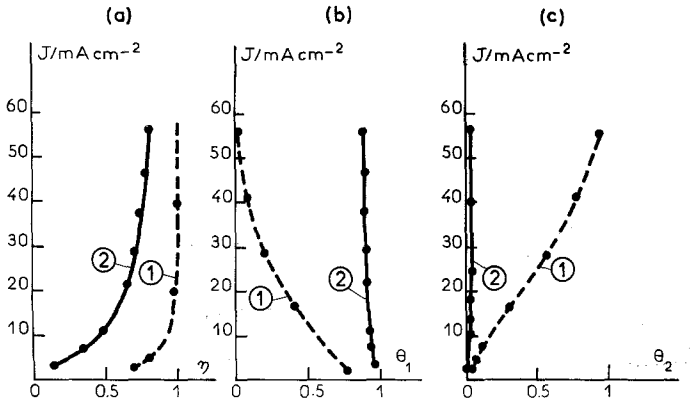

Fig. 14. Simulations of the relationships; (a) current density–efficiency; (b) current density–θ_1; (c) current density–θ_2. Curves 1 and 2 are obtained respectively with the same sets of parameters as for Curves 1 and 2 in Fig. 13a.

adsorption resists any decrease of H_{ads} coverage (θ_1) with increasing current density, as is shown by Fig. 14b. Fig. 14c shows that θ_2 (and consequently θ_3 also) varies relatively little with current density. These changes in the variations of θ_1 and θ_2 with current density are closely related to the modification in the shape of impedance diagrams observed (Fig. 6) with a pH decrease.

Conclusions

Inhibition of the irregular growth of zinc deposits, observed with three different additives, is accompanied by clear changes in the electrode kinetics. Experimentally these changes are seen as a decrease in current efficiency, a shift of current–potential curves towards more cathodic potentials, and the appearance of a capacitive loop at low frequencies, between two inductive loops on impedance diagrams. The modifications to the electrode kinetics have been interpreted in terms of a decreased autocatalytic adsorption of the cations and an enhancement of hydrogen adsorption. It was also shown that a pH decrease has a similar effect on the rates of these reactions.

Low frequency impedance measurements reveal a difference between the influence of H^+ ions and additive molecules. An acceleration of nucleation rate is observed in the presence of an additive, but not with a pH decrease. This specific influence of additive molecules on kink site renewal is closely associated with changes in deposit growth.

References

[1] F. Mansfeld and S. Gilman, *J. Electrochem. Soc.* **117** (1970) 1521.
[2] *Idem, ibid* **117** (1970) 1150.
[3] *Idem, ibid* **117** (1970) 588.
[4] J. W. Diggle and A. Damjanovic, *ibid* **119** (1972) 1649.
[5] V. V. Romanov, *Soviet Electrochem.* 7 (1971) 1400.
[6] S. Higuchi and Y. Miyake, *Denkikagaku (Electrochemistry, Japan)* **39** (1971) 896.
[7] S. Higuchi, S. Takahashi and Y. Miyake, *ibid* (1971) 522.
[8] I. N. Justinijanovic, J. N. Jovicevic and A. R. Despic, *J. Appl. Electrochem.* **3** (1973) 193.
[9] J. Bressan and R. Wiart, *ibid* 7 (1977) 505.
[10] I. Epelboin, M. Ksouri and R. Wiart, *Faraday Symposium on Electrocrystallization, Nucleation and Phase formation*, Southampton, 1977, in press.
[11] M. Ksouri, Thesis, Paris (1977).
[12] G. Giorda, *Proceedings Interfinish 76*, Amsterdam (1976).
[13] Ph. Morel, *Traitements de surface* **89** (1969) 9.
[14] *Idem, ibid* **91** (1970) 355.
[15] C. Gabrielli, M. Ksouri and R. Wiart, *Electrochim. Acta* **22** (1977) 255.
[16] I. Epelboin, M. Ksouri and R. Wiart, *J. Electrochem. Soc.* **122** (1975) 1206.
[17] J. Bressan, M. Ksouri and R. Wiart, *28th Meeting*, Druzhba (1977) Extended Abstracts, vol. 'Electrocrystallization', ISE, p. 341.
[18] T. Vitanov, A. Popov and E. Budevski, *J. Electrochem. Soc.* **121** (1974) 207.
[19] W. Allgaier and K. E. Heusler, *Z. Phys. Chem. Neue Folge* 98 (1975) 161.